Nanographene Cathode Materials for Nonaqueous Zn-ion Batteries

Shakirul M. Islam, Ryan J. Malone, Wenlong Yang, Stephen P. George, Rajendra P. Gautam, Wesley A. Chalifoux, and Christopher J. Barile*

Department of Chemistry, University of Nevada, Reno, NV 89557

*E-mail: cbarile@unr.edu

Abstract

Robust multivalent ion interaction in electrodes is a grand challenge of next-generation battery research. In this manuscript, we design molecularly-precise nanographene cathodes that are coupled with metallic Zn anodes to create a new class of Zn-ion batteries. Our results indicate that while electrodes with graphite or flat nanographenes do not support Zn-ion intercalation, the larger intermolecular spacing in a twisted peropyrene enables peropyrene electrodes to facilitate reversible Zn-ion intercalation in an acetonitrile electrolyte. While most previous Zn-ion batteries utilize aqueous electrolytes, the finding that nonaqueous Zn electrolytes can support intercalation in nanographenes is important for expanding the design space of nonaqueous multivalent batteries, which often possess higher voltages than their aqueous counterparts. Furthermore, because these nanographenes can be synthesized using a bottom-up approach via alkyne benzannulation, this work paves the way for future battery electrodes that contain other molecularly-precise nanographenes with tailored electrochemical properties.

Introduction

The advent of rechargeable Li-ion batteries in the twentieth century was a key technological breakthrough that powered the personnel electronics revolution.¹ In this century, as the scope of the battery market expands to encompass the transportation and grid storage sectors, there is an increasing need to develop new battery chemistries beyond Li-ion, with superior performance.²⁻⁸ Batteries that utilize multivalent ions such as Mg²⁺, Zn²⁺, and Al³⁺ are promising, due to their high theoretical volumetric capacities. Compared to the practical volumetric capacities of commercial Li-ion batteries (500-700 mAh cm⁻³), multivalent metal anodes have much higher theoretical volumetric capacities (3833 mAh cm⁻³, 5851 mAh cm⁻³, and 8046 mAh cm⁻³ for Mg²⁺, Zn²⁺, and Al³⁺, respectively) due to their ability to transfer more than one electron per ion.^{9, 10}

Over the last decade, much research progress has been made in designing electrolytes that facilitate reversible metal electrodeposition at multivalent metal anodes. Although some problems—such as the formation of dendrites at high current densities—remain, significant progress in the field of multivalent metal anodes has been made. Despite considerable effort, it has proved much more challenging to facilitate multivalent ion intercalation at the cathode with high capacity, high voltage, fast discharge rates, and with good reversibility. Successful multivalent ion intercalation at the anode, which is much less studied, would also be useful in obviating the lingering problems of multivalent metal anode chemistry.

In Li-ion batteries, a wide variety of materials support reversible Li⁺ intercalation with excellent electrochemical performance. Of all the systems discovered, Li⁺ intercalation in graphite anodes is probably the most studied, as the process has been known since the 1990s. ¹⁸ On the other hand, reversible multivalent ion intercalation in graphite was, until a few years ago, thought to be impossible due to strong cation- π interactions between the highly charged cations and graphite

aromatic rings.¹⁹ Recently, a few publications have reported batteries with anodes that facilitate reversible Mg²⁺ or Ca²⁺ intercalation in graphite. However, the ions that intercalate are highly solvated, which decreases the electrode's energy density. Furthermore, the interpretations of some of these results have been called into question.²⁰⁻²⁴ Nam et al. used triangular phenanthrenequinone as cathode materials for aqueous rechargeable Zn-ion batteries with high capacity. The resulting material has pores that allow for reversible Zn-ion intercalation.²⁵

To overcome the obstacles associated with multivalent intercalation into graphite, we were inspired to design multivalent battery electrodes with molecularly-precise nanographene compounds. We hypothesize that these molecules, the bottom-up synthesis of which was recently pioneered by the Chalifoux group, ²⁶⁻²⁹ can be engineered to facilitate reversible multivalent ion intercalation due to their tailorable interlayer spacing and pore sizes. The nanographenes can also be modified with chemical diversity beyond the carbon of graphite. In principle, such chemical functionality allows for enhanced intercalation properties via the tuning of electronic and steric properties.

In this manuscript, we demonstrate the first example of a battery that operates via multivalent ion intercalation into a nanographene. In particular, we construct nonaqueous Zn-ion batteries that contain a peropyrene cathode and a Zn metal anode. The high redox potential of the peropyrene (~1.5 V vs. Zn/Zn²⁺) enables it to operate as a cathode—in contrast to graphite, which traditionally functions as an anode.^{30,31} This proof-of-concept research using nanographenes opens up a new strategy for designing multivalent ion intercalation electrodes that will aid in the development of multivalent battery technologies.

Experimental

Peropyrene 1 was synthesized following a literature procedure,²⁹ and the characterization data are consistent with reported data.²⁷ Anhydrous acetonitrile was purchased from Sigma Aldrich. Anhydrous Zn(ClO₄)₂ was prepared following a literature procedure in which Zn(ClO₄)₂-6 H₂O is dried in a vacuum oven for four days at 100°C. ³² All electrochemical experiments were performed in an Ar-filled glove box with <1 ppm O₂ and <0.1 ppm H₂O. To prepare the cathode electrodes, stainless steel (alloy 316) substrates were first coated with a 15 µm thick layer of graphite using a doctor blade and a colloidal graphite dispersion (DAG EB-012, Ladd Research). The graphite was dried in a vacuum oven overnight at 80°C. The graphite serves as a conductive scaffold for the cathode material and itself does not participate in Zn ion intercalation as shown previously.³² Alternatively, Cu foil without graphite was used as a substrate. Next, 15 mg polyvinylidene fluoride (PVDF, Kynarflex 2801), 7.5 mg of Vulcan XC-72 carbon, and 7.5 mg perylene, coronene, or the peropyrene were added into a vial. Acetone (0.36 mL for voltammetry experiments or 2.5 mL for two-electrode batteries) was then added, and the resulting slurry was mixed for at least 3 hours at room temperature. The slurry was then deposited at a thickness of 15 μm using a doctor blade before it was punched into circular electrodes (4 mm in diameter).

To assemble two-electrode batteries, battery components were assembled in a polypropylene body with two stainless steel screws serving as terminals. A Zn metal (99.99%) anode followed by a glass separator (Whatman) soaked in 10 µL of electrolyte were placed on top of the bottom terminal. Then, the cathode electrode was added to the device stack followed by a stainless steel spring. The spring provides electrical connection from the top terminal to the back of the cathode.

Two pieces of Zn metal served as the reference and counter electrodes for voltammetry experiments. Scanning electron microscope (SEM) images were obtained using a Hitachi S-4700 II field emission SEM with an energy-dispersive spectrometer (EDX) at an acceleration voltage of 15kV. Matrix-assisted laser desorption/ionization time of flight (MALDI-TOF) mass spectra were recorded on a Bruker microflex MALDI-TOF spectrometer using 2,5-dihydroxybenzoic acid as the matrix. High resolution mass spectrometry with atmospheric pressure photoionization ionization (APPI) was recorded using an Agilent 6230 time of flight mass spectrometer. For all mass spectrometry experiments, a 10 µm solution of the peropyrene in a 100 mM Zn(ClO₄)₂ in acetonitrile electrolyte was first prepared. This solution was then used in a three-electrode cell with Zn reference and counter electrodes. The solution was potentiostatically cycled 100 times at 0.3 V for 10 min, followed by 1.5 V or 1.7 V for 10 min. After cycling, the solution was diluted with water and extracted with dichloromethane to separate the peropyrene from the Zn(ClO₄)₂. The organic layer was dried with anhydrous Na₂SO₄ and removed under reduced pressure to yield the peroyrene before mass spectrometry was performed.

Results and discussion

Chalifoux and coworkers have demonstrated the versatility of alkyne benzannulation for the synthesis of a broad scope of contorted nanographenes through the use of Brønsted and Lewis acid catalysts. ^{26-29, 33-36} Notable among their early work was the novel synthesis of contorted, functionalized, and processable peropyrenes. Nonaqueous solutions of these peropyrenes exhibit two reversible redox waves associated with the oxidation and reduction of the aromatic system to the corresponding radical cation and anion, respectively. ²⁹ To construct a reversible Zn²⁺ battery, a cathode containing peropyrene 1 and a Zn metal anode, sandwich an electrolyte containing Zn²⁺ (Figure 1). To evaluate this battery architecture, we chose to study electrolytes consisting of either

 $Zn(CF_3SO_3)_2$ or $Zn(ClO_4)_2$ in acetonitrile. Both of these electrolytes are known to facilitate reversible Zn electrodeposition with $\geq 99.9\%$ Coulombic efficiency. $^{32,\,34}$ There are also examples of reversible Zn^{2+} intercalation into V_3O_7 and other cathode materials using these electrolytes. $^{32,\,34}$ Lastly, acetonitrile is a desirable solvent because the peropyrene is insoluble, which allows stable electrode films to be cast. In the case of the $Zn(CF_3SO_3)_2$ electrolyte, acetonitrile also enables the electrolyte to have a much higher anodic stability $(3.5 \text{ V vs. } Zn/Zn^{2+})$ as compared to aqueous electrolytes. 38

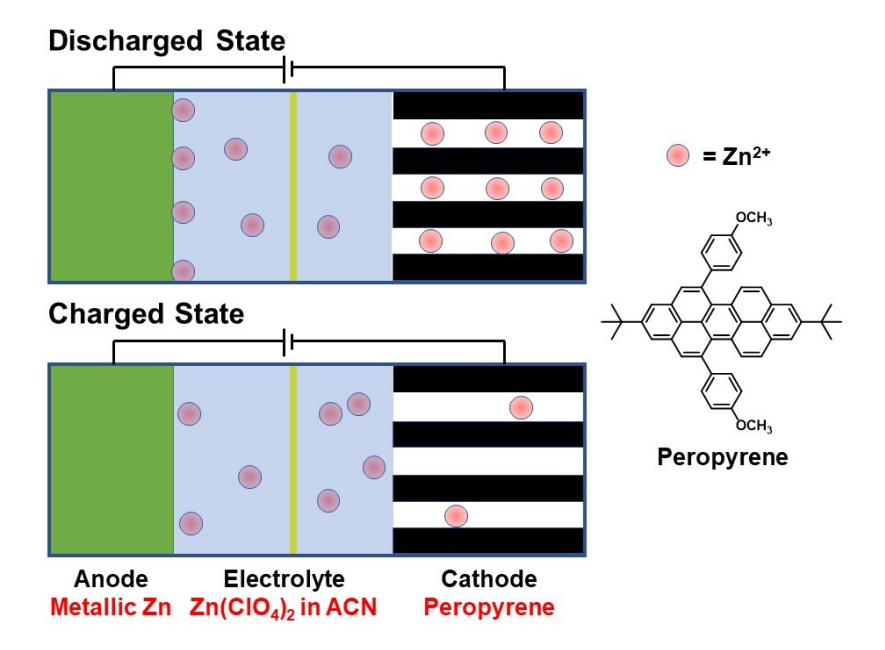


Figure 1. Schematic of a Zn^{2+} battery consisting of a peropyrene cathode and a Zn metal anode showing their nominal discharged and charged states.

The battery is constructed in a charged state with a metallic Zn anode and the peropyrene without any intercalated Zn^{2+} . Upon discharge, the Zn metal is oxidized at the anode to form Zn^{2+} , which concurrently intercalates into a film of the reduced peropyrene radical anion. Upon charge, the reverse reactions occur, in which Zn^{2+} electrodeposits to form Zn on the anode and the

peropyrene is oxidized. The peropyrene can be oxidized beyond its neutral form to a radical cation, which is charge balanced by the anion in the electrolyte (e.g. ClO₄⁻).

Before testing a full battery, we sought to understand the Zn²⁺ intercalation dynamics in the peropyrene using cyclic voltammetry (CV). We first performed CV of the peropyrene cast with Vulcan XC-72 carbon and a PVDF binder on a Cu substrate in an electrolyte containing Zn(CF₃SO₃)₂ in acetonitrile (Figure 2a, black line). At a scan rate of 0.1 mV s⁻¹, the voltammogram exhibits a cathodic peak at ~0.1 V vs. Zn/Zn²⁺ and an anodic peak at ~0.85 V vs. Zn/Zn²⁺, which we ascribe to Zn²⁺ intercalation and deintercalation, respectively. However, the large separation between the peak potentials, especially given the slow scan rate, indicates that the kinetics of Zn²⁺ intercalation are significantly impeded. A CV from a control experiment without the peropyrene in the electrode does not exhibit well-defined peaks, indicating that the voltammetric response is due to the peropyrene (Figure 2a, red line). Importantly, a CV from another control experiment using the peropyrene with tetrabutylammonium triflate (TBACF₃SO₃) instead of Zn(CF₃SO₃)₂ shows no redox behavior (Figure 2a, blue line). This result is expected, because the tetrabutylammonium ion is much larger than Zn²⁺ and presumably too large to intercalate within the pores of the peropyrene. Furthermore, an EDX spectrum of the peropyrene electrode, taken after halting the CV in the intercalated state (0 V), reveals the presence of Zn in the electrode (Figure 3a). The corresponding EDX spectrum of the electrode in the deintercalated state does not display any peaks associated with Zn (Figure 3b). Taken together, these results indicate that, although the reaction is slow, Zn²⁺ reversibly intercalates into the peropyrene using an electrolyte containing Zn(CF₃SO₃)₂ in acetonitrile.

We additionally evaluated if Zn^{2+} intercalation is feasible in the smaller nanographene molecules, coronene and perylene, the structures of which are shown on the right side of Figure 2.

Unlike the peropyrene, which possesses a twisted structure, coronene and perylene are relatively flat molecules. The smaller interlayer spacing of these molecules should make Zn²⁺ intercalation into these structures more difficult. Indeed, the CVs of electrodes with coronene (Figure 2, purple line) and perylene (Figure 2, green line) in the Zn(CF₃SO₃)₂ electrolyte confirm this hypothesis, as both CVs exhibit very low current density. The results of Figure 2a indicate that it is the unique structure of the peropyrene, with its larger interlayer spacing, that allows it to function as a reversible host for reversible Zn²⁺ intercalation. Under the same electrochemical conditions, Zn²⁺ intercalation does not occur in graphites (e.g. Vulcan XC-72) or flat nanographenes.

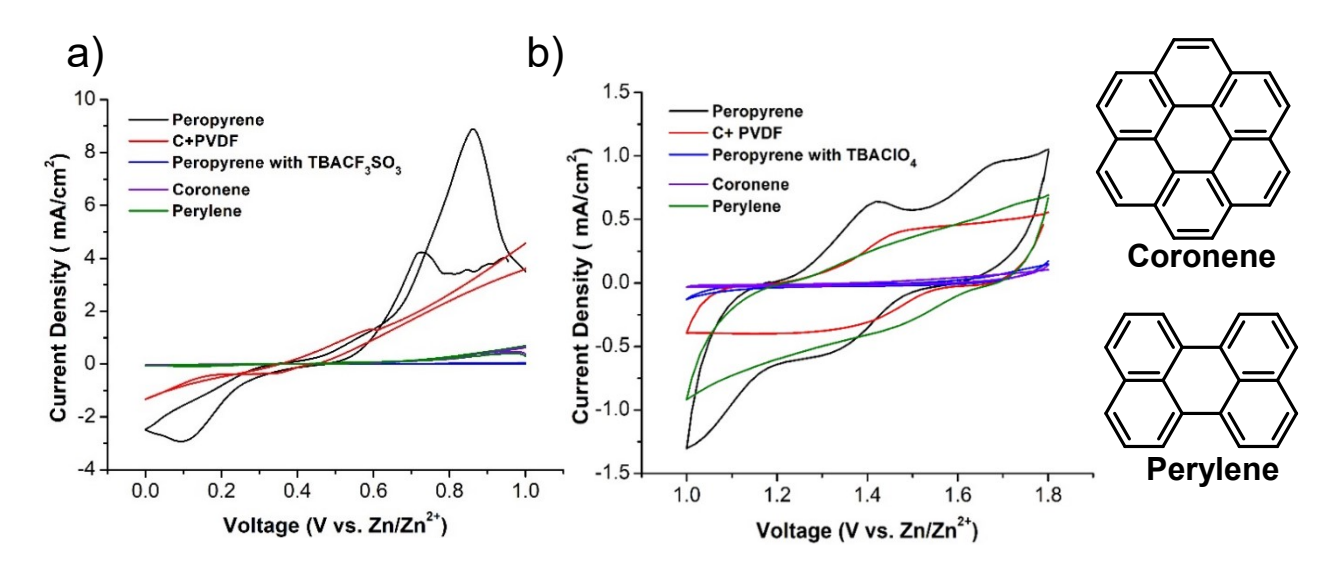


Figure 2. Cyclic voltammetry evaluating Zn^{2+} intercalation in the peropyrene (black), a control without any nanographene (red), coronene (purple), and perylene (green) cast with Vulcan XC-72 carbon and PVDF. For panel a, the electrolyte used was $100 \text{ mM } Zn(CF_3SO_3)_2$ in acetonitrile, the cathode was cast on a Cu substrate, and the scan rate was 0.1 mV s^{-1} . For panel b, the electrolyte used was $100 \text{ mM } Zn(ClO_4)_2$ in acetonitrile, the cathode was cast on a graphite-coated stainless steel substrate, and the scan rate was 50 mV s^{-1} . The blue lines indicate voltammetry with the peropyrene using an electrolyte containing $100 \text{ mM } TBACF_3SO_3$ or $TBAClO_4$ in acetonitrile.

We next performed an analogous set of voltammetry experiments using an electrolyte in which Zn(ClO₄)₂ replaces Zn(CF₃SO₃)₂ (Figure 2b). For these experiments, the electrodes were cast on graphite-coated stainless steel substrates, not Cu. Cu substrates were found to be

incompatible with the Zn(ClO₄)₂ electrolyte (Figure S1), and more information explaining this phenomenon can be found in the supporting information. Strikingly, the CV of the peropyrene electrode contains two well-defined sets of redox peaks at a much faster scan rate of 50 mV s⁻¹ (Figure 2b, black line). Based on previous literature studying the solution-phase electrochemistry of this peropyrene, ²⁹ the redox pair centered at ~1.35 V is ascribed to the neutral peropyrene and the corresponding radical anion, and the redox pair centered at ~1.65 V is assigned to the neutral peropyrene and the corresponding radical cation. The well-defined peaks at this faster scan rate indicate that Zn²⁺ intercalation dynamics are faster with the Zn(ClO₄)₂ electrolyte as compared to Zn(CF₃SO₃)₂. We hypothesize that the origin of this difference is due to greater ion dissociation in Zn(ClO₄)₂ compared to Zn(CF₃SO₃)₂. Previous reports studying Zn²⁺ intercalation in a V₃O₇ electrode, using Zn(CF₃SO₃)₂ in acetonitrile, determined that Zn²⁺ in this electrolyte remain largely ion-paired and heavily solvated, and that this solution structure resulted in slow Zn²⁺ intercalation kinetics.³⁸ For these reasons, a CV exhibiting Zn intercalation is only obtainable at a slower scan rate using the Zn(CF₃SO₃)₂ electrolyte, whereas Zn intercalation occurs faster with the Zn(ClO₄)₂ electrolyte and hence a faster scan rate can be used. CVs of the control experiments without the peropyrene (Figure 2b, red line), with tetrabutylammonium perchlorate (TBAClO₄, Figure 2b, blue line), and with coronene and perylene (Figure 2b, purple and green lines) do not exhibit welldefined peaks like the CV of the peropyrene electrode. As for the Zn(CF₃SO₃)₂ electrolyte, these experiments indicate that the molecular structure of the peropyrene is responsible for facilitating reversible Zn²⁺ intercalation. Because the redox-active species are bound to the electrodes, the electron transfer kinetics during Zn²⁺ intercalation can be calculated by dividing the peak current density in the CVs by the charge density as described previously.³⁹ Using this method, the electron transfer kinetics during Zn²⁺ intercalation are 1.2 s⁻¹, 0.2 s⁻¹, and 0.0 s⁻¹ for the peropyrene,

perylene, and coronene, respectively. These results demonstrate that faster electron transfer rates correlate with greater reversibility in the CVs. While the intermolecular spacing of the smaller and flatter coronene and perylene molecules is too small to allow for reversible Zn²⁺ intercalation, the twisted peropyrene structure is less well-packed, which enables Zn²⁺ intercalation to occur. The crystal structures of coronene and perylene indicate that these molecules have intermolecular spacings of 3.40 Å and 3.47 Å, respectively.^{40,41} In contrast, the intermolecular spacing of a structurally similar peropyrene (n-hexyl ethers replace the methyl ethers) is much larger.²⁷ Although a greater intermolecular spacing in nanographenes improves the reversibility of intercalation, less densely-packed nanographenes reduce the volumetric energy density of the battery. In future research, we will more fully explore the relationship between electronic effects, intermolecular spacing, intercalation reversibility, cell voltage, and volumetric energy density. Nanographenes modified with electron-withdrawing groups may be particularly promising because they should both increase device voltage and improve intercalation kinetics.

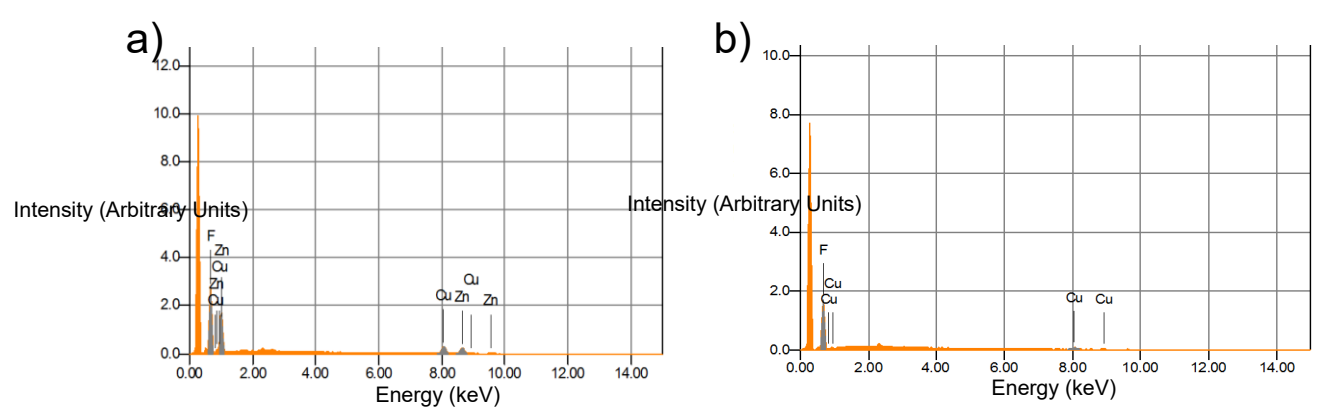


Figure 3. Energy-dispersive X-ray spectra of the peropyrene cathode cast on Cu foil in its intercalated (a) and deintercalated (b) states using an electrolyte containing Zn(CF₃SO₃)₂ in acetonitrile at a scan rate of 0.1 mV s⁻¹.

To probe the larger scale structure of peropyrene in the electrode composites, we used SEM. Figure 4a displays a SEM image of the peropyrene electrode as cast with Vulcan XC-72 carbon and PVDF binder. The rod-like structures (yellow arrows) are assigned to the peropyrene

because they are not present in SEM images of the electrodes without the peropyrene (Figure 4b). Although their exact mechanism of formation is unclear, the rod-like peropyrene structures may exist due to aggregates stabilized by π - π stacking interactions, both between adjacent peropyrene molecules and peropyrene and the carbon in the Vulcan XC-72 support.

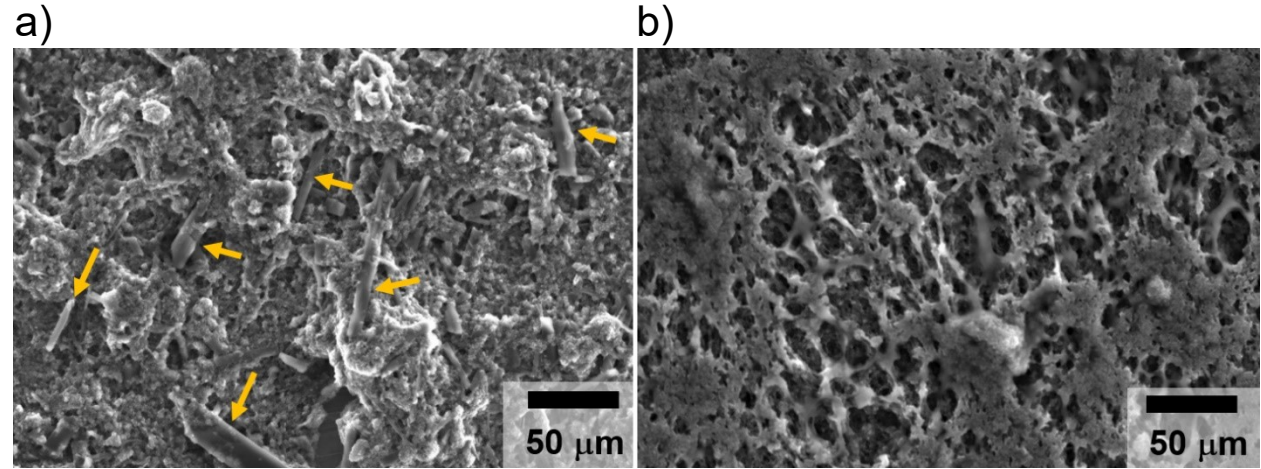


Figure 4. SEM images of electrodes with Vulcan XC-72 carbon, PVDF, and with (a) and without (b) the peropyrene. The yellow arrows in image a point to examples of the rod-like structures in the SEM, which are not present in image b and therefore are assigned to the peropyrene.

Having established that reversible Zn^{2+} intercalation occurs facilely in the peropyrene with $Zn(ClO_4)_2$, we constructed a battery that uses the $Zn(ClO_4)_2$ electrolyte and pairs a peropyrene cathode with a Zn metal anode. The discharge-charge curves of the battery are displayed in Figure 5. The open circuit potential of the battery is ~ 1.6 V, which corresponds well with the voltage of the redox peaks of the peropyrene as determined by CV (Figure 2b, black line). Based on the molar mass of the peropyrene (650.32 g mol⁻¹) and the capacity for each peropyrene to store 2 e⁻ by cycling between the radical cation, neutral, and radical anion states, the theoretical capacity for the battery, which is limited by the cathode, is 82 mAhg^{-1} . The first two discharge-charge cycles of the battery (Figure 5, black and red lines) exhibit significantly higher capacities than this theoretical value. These large capacities are likely artificially inflated by a number of potential

initial side reactions in the battery such as reactions with water or O₂ impurities in the electrolyte or solid-electrolyte interface formation. Higher than theoretical initial discharge-charge capacities are common in a wide range of battery chemistries including Zn-ion batteries.¹⁴ From the third to fifth cycles, however, the charge and discharge curves begin to stabilize near the theoretical values. Although the discharge curves begin near the open circuit potential of 1.6 V, they steadily decrease through device discharging until the cutoff voltage of 0.3 V is reached. Because the overpotentials associated with Zn electrodissolution at the anode are known to be low, 32 this behavior indicates there is significant overpotential associated with Zn²⁺ intercalation at the cathode. Discharge curves were performed at a current of 100 mA g⁻¹, which based on the battery's theoretical capacity, gives a rate of 1.2 C. In contrast, the charge curves were performed at a current of 500 mA g⁻¹ or a rate of 6 C. Even at this faster rate, the charge curves exhibit much less overpotential than the discharge curves (Figure 5b). For the majority of the capacity of the charge curves, the voltage ranges from 1.2-1.7 V, which is the same range that the redox peaks are observed in the peropyrene CV (Figure 2, black line). The lower overpotential associated with charging indicates that Zn²⁺ deintercalation is kinetically more favorable than Zn²⁺ intercalation. The fast deintercalation kinetics allow the battery to charge rapidly, which is an advantageous attribute of this battery chemistry.

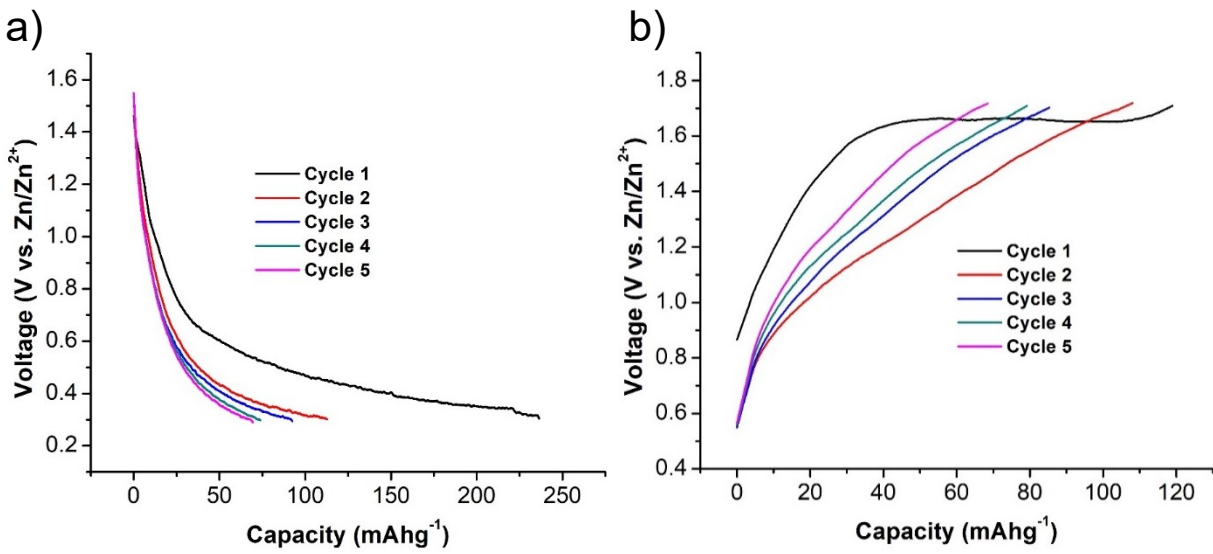


Figure 5. Discharge (a) and charge (b) curves of a Zn-ion battery with the peropyrene cathode, a Zn metal anode, and an electrolyte containing $Zn(ClO_4)_2$ in acetonitrile. Discharge and charge rates were 100 mA g^{-1} and 500 mA g^{-1} , respectively. The discharge and charge cutoff voltages were 0.3 V and 1.7 V, respectively.

Further discharge-charge curves of the battery beyond cycle 5 are shown in Figure S2, and the black line in Figure 6 plots the capacity of the battery over the course of 100 cycles. The data indicate that the capacity of the battery steadily decreases during cycling. Degradation during cycling is also evidenced by the less than 100% Coulombic efficiency of the device (Figure S3). From cycles 10-100, the Coulombic efficiency ranges between 89% and 94%. Importantly, a control experiment cycling a battery using a cathode with Vulcan XC-72 carbon and PVDF without the peropyrene indicates that this battery possesses a capacity less than 10 mAh g⁻¹ throughout cycling (Figure 6, red line and Figure S4). This experiment proves that the peropyrene is responsible for the enhanced capacity of the Zn-peropyrene battery.

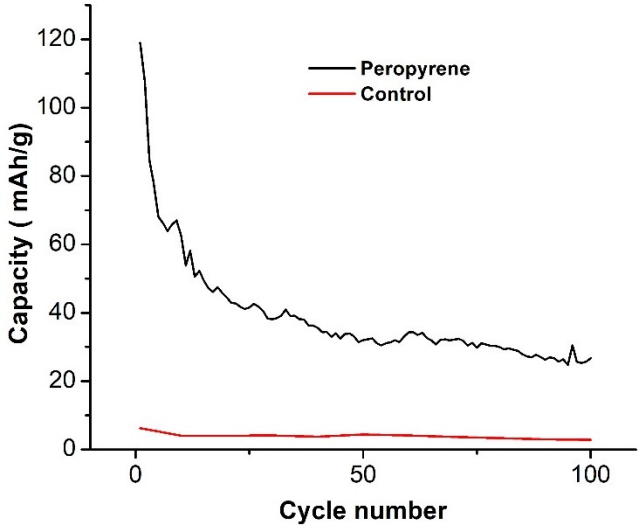


Figure 6. Capacity as a function of cycle number of Zn-ion batteries with a cathode cast using Vulcan XC-72 carbon and PVDF with (black) and without (red) the peropyrene. The discharge and charge cutoff voltages during each cycle were 0.3 V and 1.7 V, respectively.

To interrogate the origin of capacity fade during battery cycling, we performed mass spectrometry experiments of the peropyrene after cycling. A MALDI-TOF spectrum of the peropyrene after potentiostatic cycling in the Zn(ClO₄)₂ in acetonitrile electrolyte using an oxidative potential of 1.7 V indicates that the peropyrene degrades during cycling (Figure 7, red line). Many peaks higher than the theoretical m/z value for peropyrene (650.32) are observed. These peaks can be ascribed to oxidized and oligomerized peropyrene species and their fragmentation peaks. For example, the peak with a m/z value of 666 is ascribed to a singly oxidized peropyrene species, while the peaks with m/z values of 1300 and 1948 are due to peropyrene dimers and trimers, respectively. These results indicate that the peropyrene is not stable at 1.7 V, which is the cutoff voltage used in the battery cycling experiment. Therefore, the degradation of the peropyrene at this oxidative potential is likely the origin of the capacity deterioration during battery cycling.

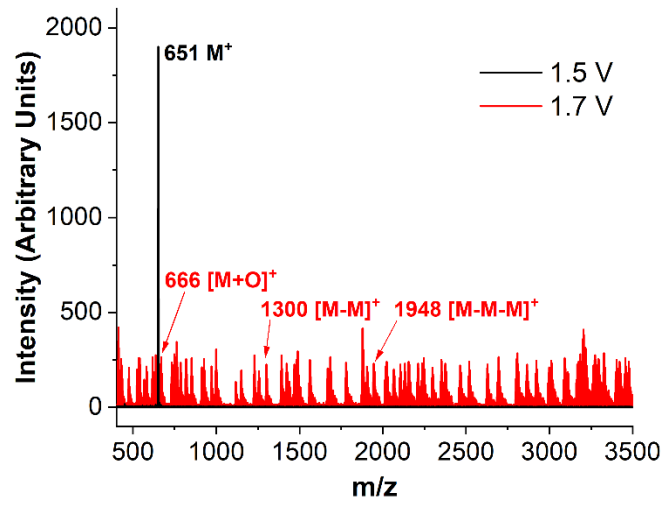


Figure 7. Positive-mode MALDI mass spectra of the peropyrene after 100 cycles using an oxidation voltage of 1.5 V (black) and 1.7 V (red). The M⁺, [M+O]⁺, [M-M⁺], and [M-M-M]⁺ labels correspond to the parent peropyrene, oxidized peropyrene, dimer, and trimer, respectively.

After determining that the peropyrene oxidatively degrades at 1.7 V vs. Zn/Zn²⁺, we used MALDI-TOF spectrometry to analyze the peropyrene cycled using a lower voltage of 1.5 V. At this lower voltage, the mass spectrum displays no evidence of oxidative degradation of the peropyrene. Instead, only one intense peak at a m/z value of 651 is present in the spectrum due to the parent peropyrene ion (Figure 7, black line). According to the CV data presented earlier (Figure 2b, black line), at the lower voltage of 1.5 V vs. Zn/Zn²⁺, the peropyrene exists in its neutral form, while at 1.7 V, the peropyrene is converted to the radical cation. The MALDI-TOF data indicate that while the neutral form of the peropyrene is stable during cycling, the radical cation is not. This interpretation is further confirmed by high-resolution APPI TOF mass spectra (Figure S5). The spectrum for the compound cycled at 1.5 V possesses the expected m/z value for the undegraded peropyrene at 650.32, while the spectrum for the peropyrene cycled at 1.7 V does not.

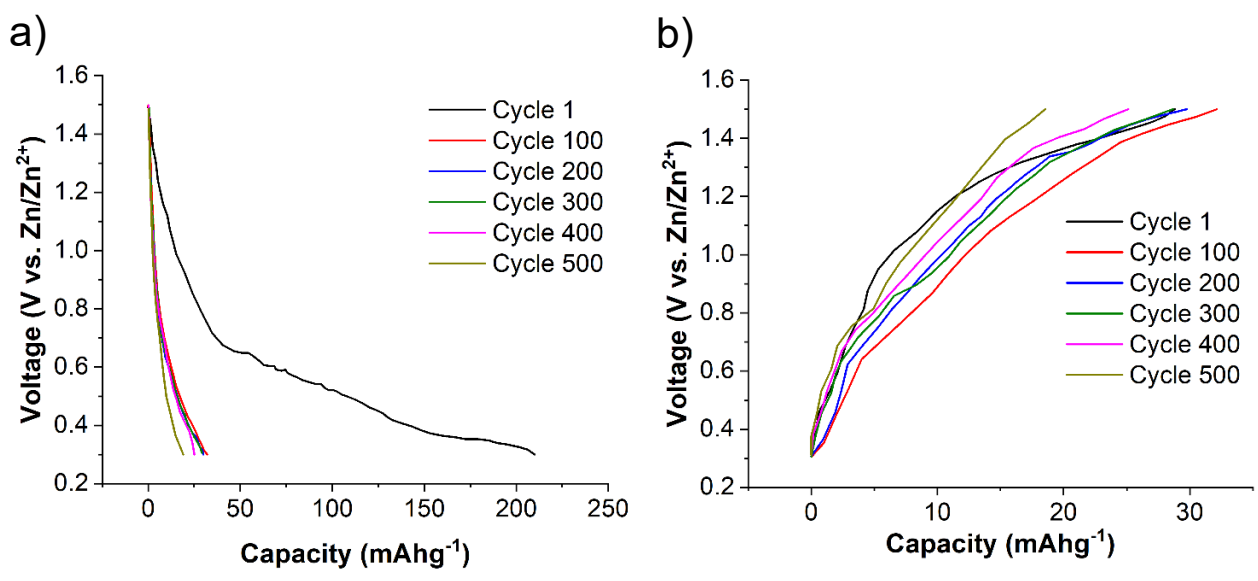


Figure 8. Discharge (a) and charge (b) curves of a Zn-ion battery with the peropyrene cathode, a Zn metal anode, and an electrolyte containing Zn(ClO₄)₂ in acetonitrile. Discharge and charge rates were 100 mA g⁻¹ and 500 mA g⁻¹, respectively. The discharge and charge cutoff voltages were 0.3 V and 1.5 V, respectively.

Based on these mass spectrometry results demonstrating the stability of the peropyrene at 1.5 V, we hypothesized that the battery cycle life could be improved by implementing a cutoff voltage of 1.5 V during device charging. Indeed, cycling results with a 1.5 V cutoff voltage indicate much improved battery cyclability vis-à-vis the 1.7 V cutoff voltage experiment (Figure 8). During discharge, the first cycle capacity is high (> 200 mAhg⁻¹) due to irreversible side reactions during battery initialization (Figure 8A, black line). The charge capacities and subsequent discharge capacities, however, exhibit values in line with theoretical capacities. During cycling, the charge capacity of the battery slowly decreases from an initial value of about 30 mAhg⁻¹ (Figure 9). Even after 300 cycles, the battery still possesses a capacity of about 30 mAhg⁻¹, which is the capacity the battery decreased to after only 100 cycles using a cutoff voltage of 1.7 V. Therefore, the cycle life of the battery is increased at least threefold by avoiding the degradative chemistry observed when the peropyrene is oxidized to its radical cation. We note that the theoretical energy density

of the battery decreases to 41 mAhg⁻¹ at this lower cutoff voltage of 1.5 V compared to 82 mAhg⁻¹ at 1.7 V because the peropyrene only facilitates the transfer of one electron as opposed to two.

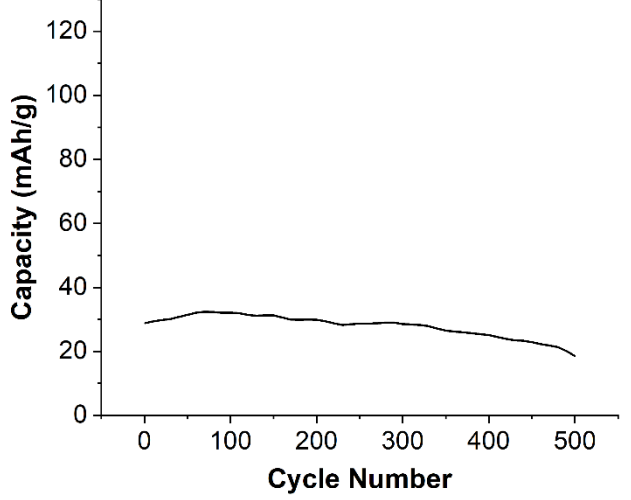


Figure 9. Charge capacity as a function of cycle number of a Zn-ion battery with a cathode cast using Vulcan XC-72 carbon and PVDF with the peropyrene. The discharge and charge cutoff voltages during each cycle were 0.3 V and 1.5 V, respectively.

Considering the presented experimental results as a whole, we next give a unified description of the mechanistic details that dictate the performance of the Zn-peropyrene battery. When the neutral form of the peropyrene at the cathode is reduced to its radical anion during battery discharging, Zn²⁺ formed by the oxidation of the Zn metal anode intercalates into the peropyrene from the acetonitrile-based electrolytes. Zn²⁺ intercalation is faster when using Zn(ClO₄)₂ as the Zn²⁺ source as compared to Zn(CF₃SO₃)₂ because the solvation sphere around Zn²⁺ is weaker in the case of Zn(ClO₄)₂.³⁸ Furthermore, the twisted structure of the peropyrene allows for reversible Zn²⁺ intercalation during battery cycling, which does not occur for the flatter nanographenes evaluated. Lastly, if the peropyrene is oxidized to its radical cation during charging, the cycling performance of the battery is limited by oligomerization and oxidative side reactions of the peropyrene. However, these side reactions are completely avoided when the charging cutoff

voltage is made less positive, in which case the battery cycles hundreds of times with a relatively stable capacity.

Outlook and Comparisons to other Nonaqueous Zn Batteries

The performance of the Zn-peropyrene battery developed here is comparable to many other nonaqueous Zn-ion battery chemistries actively being researched. For example, Chae et al. reported a Zn-ion battery in an organic electrolyte using a hexacyanoferrate-based cathode that cycled 40 times with a capacity between 45-55 mAh g⁻¹ at a much slower rate of 0.2 C.³² Also at a slow rate of 0.2 C, Pan et al. developed a Zn-ion battery in an acetonitrile electrolyte with a spinelbased cathode that cycled 200 times with a capacity of at least 150 mAh g⁻¹.⁴² Using a cathode material containing Mo and V and an electrolyte comprised of propylene carbonate and DMSO, Kaveevivitchai et al. developed nonaqueous Zn-ion batteries that cycle 30 times at a cycling rate of about 0.1 C.43 Other nonaqueous Zn-ion battery electrode materials such as Na₃V₂(PO₄)₂F₃ exhibit even inferior cycle lives of only 10 cycles at a rate of 0.3 C.44 In comparison, the peropyrene-based battery developed here cycles at rates greater than 1 C at least 500 times with a capacity between 20-35 mAh g⁻¹. This excellent cycle life at a fast rate with a moderate capacity is analogous to the properties of graphite in Li-ion batteries, which also possesses excellent cyclability, but reduced capacities compared to other, less durable, electrode materials such as $\mathrm{Si.}^{45}$ Compared to nonaqueous Zn-ion batteries, numerous aqueous Zn-ion batteries have been developed with high capacities and outstanding cycle lives. 46 The potential benefit of nonaqueous Zn-ion batteries, however, is the expanded voltage windows of the nonaqueous solvents utilized, which ultimately could lead to the development of higher capacity batteries compared to their aqueous counterparts.

Beyond battery performance, the key innovation presented in this manuscript is the use of a molecularly-precise nanographene cathode for nonaqueous multivalent ion intercalation. Compared to aqueous systems, there are relatively few examples of reversible multivalent ion intercalation in layered cathode materials. This research introduces a new strategy to facilitate nonaqueous multivalent ion intercalation in graphitic materials. In future research, we will study the intercalation of other multivalent ions such as Mg²⁺ and Ca²⁺ in nanographenes. The variety of contorted nanographenes, including persistently chiral compounds, which can be produced using alkyne benzannulation allows us to explore alternative nanographenes to increase device performance moving forward.

Conclusions

In conclusion, we demonstrated that a peropyrene-based nanographene produced through bottom-up organic synthesis can be utilized as a cathode in non-aqueous Zn batteries when coupled with a Zn metal anode. While simple flat nanographene analogs do not facilitate reversible Zn-ion intercalation, the twisted structure of the peropyrene allows for reversible Zn-ion intercalation in a Zn(ClO₄)₂ electrolyte in acetonitrile. The peropyrene exhibits two redox peaks ascribed to transitions between the radical anion, neutral, and radical cation forms of the molecule. Mass spectrometry results indicate that while accessing the radical cation during battery cycling leads to irreversible oxidation, the battery cycles 500 times at rates greater than 1 C without any oxidative degradation when cycling between the radical anion and neutral forms. As a whole, this manuscript presents a new strategy for facilitating multivalent ion intercalation in nonaqueous electrolytes using a molecularly-precise nanographene as an intercalation host.

Acknowledgement

This research was partially supported by Research and Innovation at the University of Nevada, Reno (UNR). SEM-EDS analysis was performed in the Mackay Microbeam Laboratory at UNR, we acknowledge J. Desormeau for his kind assistance. C. J. B. acknowledges the National Science Foundation for financial support through a CAREER Award (CHE-2046105). W. A. C. acknowledges the National Science Foundation for financial support through a CAREER Award (CHE-1555218).

Competing Interests

C. J. B. and W. A. C. have filed a provisional patent associated with this work. The other authors declare no competing financial interest.

Additional Information

Supplementary Information The online version contains supplementary information

References

- 1. J. B. Goodenough and K.-S. Park, J. Am. Chem. Soc. 135, 1167 (2013).
- 2. A. Ponrouch, and M. R. Palacín, *Philos. T. Rov. Soc. A.* **377**, 20180297 (2019).
- 3. M. Walter, M. V. Kovalenko and K. V. Kravchyk, New. J. Chem. 44, 1677 (2020).
- 4. J. M. Tarascon and M. Armand, *Nature*. **414**, 359 (2001).
- 5. Y. Zhao, Y. Zhu, and X. Zhang, *InfoMat.* 2, 237 (2019).
- 6. Y. Gao, H. Yang, X. Wang, Y. Bai, N. Zhu, S. Guo, L. Suo, H. Li, H. Xu, and C. Wu, *Chem. Sus. Chem.* 13, 732 (2020).
- 7. H. J. Liang, Z. Y. Gu, X. Y. Zheng, W. H. Li, L. Y. Zhu, Z. H. Sun, Y. F. Meng, H. Y. Yu, X. K. Hou, and X. L. Wu, *J. Energy Chem.* **59**, 589 (2021).
- 8. W. H. Li, H. J. Liang, X. K. Hou, Z. Y. Gu, X. X. Zhao, J, Z. Guo, X. Yang, and X. L. Wu, *J. Energy Chem.* **50**, 416 (2020).
- 9. N. Nitta, F. Wu, J. T. Lee, J. T. and G. Yushin, Mater. Today. 18, 252 (2015).
- 10. D. Selvakumaran, A. Pan, S. Liang, and G. Cao, J. Mat. Chem. A. 7, 18209 (2019).
- 11. R. Deivanayagam, B. J. Ingram, and R. Shahbazian-Yassar, *Energy Storage Mater.* **21**, 136 (2019).
- 12. Y. Jie, Y. Tan, L. Li, Y. Han, S. Xu, Z. Zhao, R. Cao, X. Ren, F. Huang, Z. Lei, G. Tao, G. Zhang, and S. Jiao, *Angewante. Chemie. Int. Ed.* **59**, 12689 (2020).

- 13. Z. Li, O. Fuhr, M. Fichtner, and Z. Zhao-Karger, Energ. Environ. Sci. 12, 3496 (2019).
- 14. S. Huang, J. Zhu, J. Tian, and Z. Niu, Z. Chem. Eur. J. 25, 14480 (2019).
- 15. H. Tang, Z. Peng, L. Wu, F. Xiong, C. Pei, Q. An, and L. Mai, *Electrochem. Energ. Rev.* 1, 169 (2018).
- 16. A. Parija, Y. Liang, J. L. Andrews, L. R. D. Jesus, D. Prendergast, and S. Banerjee, *Chem. Mater.* **28**, 5611 (2016).
- 17. H. Li, N. L. Okamoto, T. Hatakeyama, Y. Kumagai, F. Oba, and T. Ichitsubo, *Adv. Energ. Mater.* **8**, 1801475 (2018).
- 18. R. Yazami, and P. A. Touzain, *J. Power Sources.* **9**, 365 (1983).
- 19. Y. Li, Y. Lu, P. Adelhelm, M. M. Titirici, and Y. S. Hu, Chem. Soc. Rev. 48, 4655 (2019).
- 20. C. God, B. Bitschnau, K. Kapper, C. Lenardt, M. Schmuck, F. mautner, and S. Koller, *RSC Adv.* 7, 14168 (2017).
- 21. D. Kim, S. C. Jung, S. Ha, Y. Kim, Y. Park, J. H. Ryu, Y. Han, and K. T. Lee, *Chem. Mater.* **30**, 3199 (2018).
- 22. J. Park, Z. Xu, G. Yoon, S. K. Park, J. Wang, H. Hyun, H. Park, J. Lim, Y. Ko, Y. S. Yun, and K. Kang, *Adv. Mater.* **32**, 1904411 (2020).
- 23. S. J. R. Prabakar, A. B. Ikhe, W. B. Park, K. C. Chung, H. Park, K. J. Kim, D. Ahn, J. S. Kwak, K. S. Sohn, and M. Pyo, *Adv. Sci.* **6**, 1902129 (2019).
- 24. J. Park, Z. L. Xu, and K. Kang, Front. Chem. 8, 1 (2020).
- 25. K. W. Nam, H. Kim, Y. Beldjoudi, T. W. Kwon, D. J. Kim, and J. F. Stoddart, *J. Am. Chem. Soc.* **142**, 2541 (2020).
- 26. A. D. Senese, and W. A. Chalifoux, *Molecules*. 24, 118 (2019).
- 27. W.Yang, J. H. S. K. Monteiro, A. de Bettencourt-Dias, V. J. Catalano, and W. A. Chalifoux, *Angew. Chemie. Int. Ed.* **55**, 10427 (2016).
- 28. W. Yang, G. Longhi, S. Abbate, A. Lucotti, M. Tommasini, C. Villani, V. J. Catalano, A. O. Lykhin, S. A. Varganov, and W. A. Chalifoux, *J. Am. Chem. Soc.* **139**, 13102 (2017).
- 29. W. Yang, G. Longhi, S. Abbate, A. Lucotti, M. Tommasini, C. Villani, V. J. Catalano, A. O. Lykhin, S. A. Varganov, and W. A. Chalifoux, *Org. Chem. Front.* **5**, 2288 (2018).
- 30. A. Yoshino, Angew. Chemie. Int. Ed. 51, 5798 (2012).
- 31. Y. P.Wu, C. Jiang, C. Wan, and R. Holze, J. Power Sources. 111, 329 (2002).
- 32. M. S. Chae, J. W. Heo, H. H. Kwak, H. Lee, and S. T. Hong, *J. Power Sources.* **337**, 204 (2017).
- 33. W.Yang, J. H. S. K. Monteiro, A. d. Bettencourt-Dias, and W. A. Chalifoux, *Can. J. Chem.* **95**, 341-345 (2017).
- 34. S. D. Han, N. N. Rajput, X. Qu, B. Pan, M. He, M. S. Ferrandon, C. Liao, K. A. Persson, and A. K. Burrell, *ACS. Appl. Mater. Inter.* **8**, 3021 (2016).
- 35. W.Yang, R.Bam, V. J. Catalano, and W. A. Chalifoux, *Angew. Chemie. Int. Ed.* 57, 14773 (2018).
- 36. W.Yang, J. H. S. K. Monteiro, A. de Bettencourt-Dias, V. J. Catalano, and W. A. Chalifoux, *Chem. Eur. J.* **25**, 1441 (2019).
- 37. K. M. Magiera, V. Aryal, and W. A. Chalifoux, Org. Biomol. Chem. 18, 2372 (2020).
- 38. D. Kundu, S. H. Vajargah, L. Wan, B. Adams, D. Prendergast, and L. F. Nazar, *Energ. Environ. Sci.* 11, 881 (2018).
- 39. A. L. Eckermann, D. J. Feld, J. A. Shaw, and T. J. Meade, Coord. Chem. Rev. 254, 1769 (2010).
- 40. J. M. Robertson and J. G. White, *J. Chem. Soc.* **0**, 607 (1945).
- 41. D. M. Donaldson, J. M. Robertson, and J. White, Proc. R. Soc. Lond. 220, 311 (1953).

- 42. C. Pan, R. Zhang, R. G. Nuzzo, and A. A. Gewirth, Adv. Energy Mat. 8, 1800589 (2018).
- 43. W. Kaveevivitchai and A. Manthiram, J. Mater. Chem. A. 4, 18737 (2016).
- 44. M. J. Park and A. Manthiram, ACS. Appl. Energy Mater. 3, 5015 (2020).
- 45. S. Chae, S. Choi, N. Kim, J. Sung, and J. Cho, Angew. Chemie. Int. Ed. 59, 110 (2020).
- 46. P. Ruan, S. Liang, B. Lu, H. J. Fan, and J. Zhou, *Angew. Chemie. Int. Ed.* **61**, e202200598 (2022).